Electrophoresis

WILEY-VCH

ELECTROPHORESIS

RESEARCH ARTICLE

Enhanced Staining and Imaging of Electrophoretically Separated Membrane Proteins Solubilized by SMA/DIBMA Polymers

Nilabh Saksena[1] | Mahipal S. Rao[1] | Spencer C. Moore[1] | Sree Kavya Penneru[1] | Wanxin Zhao[2] | Nathan G. Brady[1] | Barry D. Bruce[1,3,4]

[1]Department of Biochemistry & Cellular and Molecular Biology, University of Tennessee, Knoxville, Tennessee, USA | [2]Webb School of Knoxville, Knoxville, Tennessee, USA | [3]Department of Microbiology, University of Tennessee, Knoxville, Tennessee, USA | [4]Department of Chemical and Biomolecular Engineering, University of Tennessee, Knoxville, Tennessee, USA

Correspondence: Barry D. Bruce (bbruce@utk.edu)

Received: 6 August 2025 | **Revised:** 21 December 2025 | **Accepted:** 23 December 2025

Keywords: detergents | electron transport complexes | electrophoresis | membrane proteins | mitochondria | protein gels | thylakoid

ABSTRACT

Recent advances in membrane protein biochemistry have enabled the isolation of complexes in detergent-free, near-native states using synthetic amphipathic copolymers such as styrene-maleic acid (SMA) and diisobutylene maleic acid (DIBMA). However, these polymers often interfere with conventional protein detection methods, particularly in SDS-PAGE and Clear Native PAGE (CN-PAGE), hindering visualization and quantification. Here, we systematically evaluated 15 staining and detection methods—including Coomassie Brilliant Blue, silver, zinc, copper, Ponceau S, and SYPRO fluorescent dyes—on proteins solubilized by 13 different agents, including detergent *n*-dodecyl-*β*-D-maltoside (DDM), five SMA variants, and three DIBMA variants, from bovine heart mitochondria and cyanobacterial thylakoids. A photochemical, stain-free detection method using trichloroethanol (TCE) and UV activation proved to be optimal. This method covalently labels solvent-accessible tryptophan and tyrosine residues, generating robust fluorescence signals that are unaffected by polymer interference. TCE-modified proteins display dual emission peaks at ~460 nm and a shoulder near 490 nm, likely corresponding to tyrosine and tryptophan adducts, respectively. The polymer-insensitive nature of TCE labeling allows sharp band resolution, particularly for low molecular weight proteins, and is compatible with high-throughput microplate analysis. This approach significantly enhances the qualitative and quantitative assessment of membrane proteins solubilized in polymer nanodiscs, enabling improved detection sensitivity, reduced background, and precise visualization of subunits. By facilitating accurate biochemical characterization of membrane proteins in their native-like lipid environments, this method provides a powerful tool for structural and functional proteomics across diverse biological systems.

1 | Introduction

Membrane proteins constitute approximately one-third (27%) of the human proteome and are crucial to numerous biological processes; yet, they have been notoriously difficult to study [1–4]. The primary challenge lies in extracting membrane protein complexes from their native lipid environment and forcing them into an unnatural solvated state, followed by a crystalline environment. Traditionally, detergents have been used for the isolation and purification of membrane proteins [1–4]. These amphipathic molecules form micelles that provide a hydrophobic environment surrounding membrane proteins [5]. However, detergents have limitations: They fail to accurately replicate lipid-protein interactions essential for maintaining protein function and structure

and can thereby lead to protein denaturation [6–8]. In recent years, styrene-maleic acid (SMA) copolymers have emerged as a promising alternative for membrane protein extraction [9–16]. These polymers solubilize membranes by forming nanodiscs that encapsulate lipid and protein components, thereby preserving the proteins' native conformation and lipid interactions [17, 18]. Similarly, diisobutylene maleic acid (DIBMA) copolymers have also been shown to be effective at solubilizing membranes [19–23]. However, a common challenge with SMA- and DIBMA-solubilized proteins is the significant background interference in the commonly used electrophoretic methods, which makes protein visualization challenging and further exacerbates the detection of low-molecular-weight proteins [24, 25].

We have developed and tested numerous novel and commercially available polymers for their ability to solubilize membrane complexes from thylakoids. Previous studies have demonstrated the utility of SMA copolymers in isolating proteins from cyanobacterial and chloroplast thylakoid membranes [12, 16, 26–28] and the interaction of these copolymers with thylakoid membrane mimetics, which are dynamic and rich in galactolipids like monogalactosyldiacylglycerol (MGDG), digalactosyldiacylglycerol (DGDG), and the anionic sulfolipid sulfoquinovosyldiacylglycerol (SQDG) [29–32]. Although thylakoids are among the most extensively studied and abundant membranes [33], their unique composition sets them apart from other membrane types, which are primarily composed of phospholipids. To broaden our understanding, we extended our studies to include the inner membrane of mitochondria isolated from fresh bovine heart tissue. This membrane, which is also involved in electron transport, is well-studied and rich in phospholipids, comprising 38%–45% phosphatidylcholine (PC), 32%–39% phosphatidylethanolamine (PE), 14%–23% cardiolipins, and 2%–7% phosphatidylinositols [34].

By comparing thylakoid membranes to mitochondrial membranes, we evaluated the effectiveness of 13 different polymers across the two well-studied membrane systems, which have significantly different lipid compositions. In our study, we specifically chose cyanobacterial TS-821 thylakoid membranes and bovine heart mitochondrial membranes to compare the solubilization efficacy of the following SMA and DIBMA copolymers—SMA 1440, SMA 2625, SMA 30010, SMA 17352, SMA PRO 10235 (from Cray Valley, formerly of Total, acquired by Polyscope), Sulfo-SMA, SMA BZ25, SMA BZ30, SMA BZ35, SMA BZ40, DIBMA 10, DIBMA 12, and Sulfo-DIBMA (from Cube Biotech). Given its lack of background interference in SDS-PAGE, we also used the detergent *n*-dodecyl-*β*-D-maltoside (DDM) as a control. Following membrane solubilization and SDS-PAGE, we assessed fourteen protein stains for their impact on polymer-induced background interference, including five Coomassie Brilliant Blue (CBB) stains, five fluorescent SYPRO stains, as well as silver, zinc, copper, and Ponceau S stains. Additionally, we evaluated a stain-free technique using gels containing the trihalo compound 2,2,2-trichloroethanol (TCE) [35]. Unlike traditional protein detection methods, TCE gels enable immediate protein visualization after SDS-PAGE through short UV photoactivation [36]. This approach eliminates background interference while enabling high-sensitivity detection of proteins solubilized using SMA and DIBMA polymers. The development and optimization of this method would allow its application to custom gel formulations with variable acrylamide/bis-acrylamide concentrations—often required for improved resolution of membrane protein complexes. Furthermore, preliminary experiments have shown its potential to be readily adapted to other electrophoretic separation techniques, such as Clear Native PAGE (CN-PAGE).

In addition to improving sensitivity and flexibility, this approach offers significant cost savings by reducing dependence on commercially available precast stain-free gels. Together, we believe that implementing this staining protocol will substantially minimize background noise, which currently hampers protein detection, thereby advancing the analytical capabilities of membrane structural biology.

2 | Materials and Reagents

Polymers: The following polymers were generously provided by Cray Valley to B.D.B.: SMA 1440, SMA 2625, SMA 17352, SMA 30010, and SMA PRO 10235. The following polymers were purchased or provided as a gift from Cube Biotech: Sulfo-SMA, SMA BZ25, SMA BZ30, SMA BZ35, SMA BZ40, DIBMA 10, DIBMA 12, and Sulfo-DIBMA.

Detergents: DDM was purchased from Glycon Biochemicals.

Electrophoresis gels and MW standards: Precision Plus Dual Color Protein Standard, Precision Plus Unstained Protein Standard, and Any kD Mini-PROTEAN TGX Precast Protein Gels (Bio-Rad).

Misc. chemicals: Imidazole, $ZnCl_2$, $CuCl_2$, TCE, ethanol, methanol, glacial acetic acid, acetone, trichloroacetic acid (TCA), formaldehyde, $Na_2S_2O_3$, $AgNO_3$, Na_2CO_3, DTT, glycerol, bromophenol blue (BPB), APS, TEMED, acrylamide, SDS, glycine, Tris, HCl, sucrose (Sigma).

Stains: The following stains were purchased: InstantBlue Coomassie (Abcam); Coomassie Fluor Orange, Coomassie R-250, GelCode Blue, SimplyBlue SafeStain, SYPRO Orange, SYPRO Red, SYPRO Ruby, SYPRO Tangerine (Thermo Fisher); Ponceau S (Acros Organics).

3 | Methods

3.1 | Cyanobacteria Growth

Chroococcidiopsis TS-821 was cultured in BG-11 medium at 45°C with aeration, growing the cyanobacterial cells photoautotrophically in a 25-L flat panel airlift photobioreactor (photosystem I [PSI], Photon Systems Instruments, Czech Republic) under dual LED illumination (red and white). A proprietary air and CO_2 filtration system provided vertical aeration. Once the cells reached an optical density at 680 nm (OD680) of approximately 0.8, we harvested them using a floor model centrifuge and stored the resulting cell pellets at −80°C for future experiments.

3.2 | Thylakoid Membrane Isolation

We harvested cells during the late log phase and either stored the cell pellets at −80°C or immediately washed them in Buffer A

(50 mM MES–NaOH, pH 6.5, 5 mM $CaCl_2$, and 10 mM $MgCl_2$) for isolation of the thylakoid membrane. After pelleting the cells, we resuspended the pellets in Buffer A containing 500 mM sorbitol and then lysed them using an LM10 microfluidizer (Microfluidics International Corp., Westwood, MA). Thylakoid membranes were isolated by centrifugation at 180 000 × *g* for 1 h. We then resuspended the pellets in Buffer A with 12.5% glycerol and stored them at −80°C.

We measured chlorophyll concentration using spectrophotometry. For DDM isolation of PSI, we washed the isolated thylakoid membranes three times using Dounce homogenization and centrifugation at 180 000 × *g* in Buffer A. For polymer isolation of PSI, we used Buffer S (50 mM Tris–Cl, 125 mM KCl, pH 9.5 at room temperature). After the final wash, the thylakoid membrane fragments were adjusted to a 1 mg/mL chlorophyll concentration before starting solubilization trials.

3.3 | Bovine Mitochondria Isolation

We obtained fresh bovine hearts immediately after the humane euthanization of the cattle at a local slaughterhouse. We transported the hearts on ice and processed them within 60 min of termination. After carefully removing visible fat using a scalpel, we homogenized the tissue and then centrifuged the homogenate to separate the fat and non-homogenized tissue. We isolated the mitochondrial fraction by loading the tissue slurry onto a 35%–50% Percoll step gradient and centrifuging at 40 000 × *g*. Finally, we collected the mitochondrial fraction and stored it at −80°C for future use.

3.4 | Thylakoid Membrane Solubilization

We dissolved the polymers in double-distilled water (ddH_2O) to a final concentration of 1.25% (w/v). Thylakoid membrane samples were mixed with these polymer solutions and incubated on a shaker at 200 rpm for 1 h at 37°C. After incubation, the samples were ultracentrifuged at 47 000 rpm for 30 min at 4°C. The supernatants containing the solubilized protein–lipid complexes were carefully collected and stored for subsequent analysis.

3.5 | Mitochondrial Membrane Solubilization

We thawed the frozen mitochondrial membranes to 4°C and adjusted the protein concentration to 2.5 mg/mL. The polymers were dissolved in deionized water (diH_2O) to reach a final concentration of 1.25% (w/v). Membrane samples were incubated with the polymer solutions on a shaker at 200 rpm for 1 h at 37°C. Following incubation, the samples were ultracentrifuged at 47 000 rpm for 30 min at 4°C. The resulting supernatants were collected for use in downstream experiments.

3.6 | SDS-PAGE Sample Preparation

Protein samples were solubilized using a 4× sample buffer containing Tris–HCl: 0.2 M, pH 6.8, 8% SDS, 400 mM DTT, and 0.01% BPB. To each solubilized membrane sample (6 µL), we added 2 µL of 4× sample buffer, followed by vortexing. The samples were then denatured by incubation in a water bath at 50°C for 10 min. After denaturation, the samples were briefly centrifuged at 20 000 rpm using a microfuge. We used Bio-Rad Precision Plus Unstained Protein Standards in stain-free and fluorescent gels and Bio-Rad Precision Plus Dual Color Protein Standards in the other gels for size estimation. All MW standards were treated under the same conditions as the experimental samples, including the use of a 4× sample buffer and the denaturation protocol.

3.7 | Protein Electrophoresis

Electrophoresis was performed using optimized Tris–glycine and stain-free gel recipes. We used a custom 16-well comb to cast stacking gels, which provided 15 sample lanes and one protein standard lane. The Tris–glycine gradient gels comprised a 10%–20% resolving gel and a 4.8% stacking gel. For the resolving gels, we prepared the 10% portion with 10% w/v sucrose and the 20% portion with 20% w/v sucrose. Electrophoresis was run at 70 V for 20 min to resolve the stacking gel, followed by a step protocol of 100 V for 1 h and 150 V for ∼1 h or until the dye front reached the end of the gel.

For the stain-free gels, we added TCE to the resolving gel mixture to a final concentration of 0.5%. Precast TGX gels were run at a constant voltage of 150 V for 1 h.

3.8 | Stain-Free CN-PAGE

A 3%–8% T acrylamide gradient gel was cast using a 37.5:1 acrylamide-to-bisacrylamide ratio. The gel solution was supplemented with 0.5% TCE to enable stain-free protein visualization. Samples were mixed 1:1 with native sample buffer (50 mM Tris, 150 mM NaCl, pH 7.0, 10% glycerol, and 0.02% BPB). Approximately 1 µg of total protein from solubilized chloroplast membranes (CM) was loaded per well. Electrophoresis was performed at a constant voltage of 75 V for 3 h at 4°C. Following the run, gels were activated under UV light for 45 s in a Bio-Rad stain-free imager and visualized using the stain-free detection mode. Subsequently, gels were stained with InstantBlue Coomassie Stain (Abcam) and imaged under colorimetric settings using the same instrument.

3.9 | Fluorescence Measurements

Fluorescence experiments were performed on bovine serum albumin (BSA) and PSI. Fluorescence emission spectra were measured by exciting the samples at 310 nm, and the emission was recorded from 350 to 600 nm with a slit width of 2 nm. Cuvettes were rinsed with ethanol, methanol, and water between readings. Photoactivation was performed by mixing the sample components in a cuvette and irradiating the cuvette with UV for 15 min. For denaturation, SDS was added to the protein at 4% final concentration, and this mix was heated to 65°C for 15 min. Postheating TCE was added and then photoactivated under UV, as above. BSA was used at 0.66 mg/mL protein concentration, and PSI was used at 0.12 mg/mL protein concentration or 0.016 mg/mL chl a concentration.

3.10 | Staining Procedures

- TCE stain-free gel: Gels were cast with 0.5% TCE. After electrophoresis, UV activation was performed for 1 min using the ChemiDoc MP imaging system, followed by imaging.
- InstantBlue Coomassie: Gels were briefly rinsed with diH2O and stained with InstantBlue Coomassie for 1 h. The excess stain was removed by washing the gels with diH2O.
- GelCode Blue: Gels were washed three times with diH2O for 5 min each, followed by 1 h of staining with GelCode Blue. After staining, the gels were washed with diH2O for 1 h to remove excess stain.
- SimplyBlue SafeStain: Gels were washed three times with diH2O for 5 min each, followed by 1 h of staining with SimplyBlue SafeStain. Gels were then washed with diH2O for 1 h.
- CBB R-250: A staining solution containing 3 g/L CBB R-250, 45% methanol, and 10% glacial acetic acid was prepared and filtered. Gels were fixed overnight in a solution of 50% methanol and 10% acetic acid, stained for 2 h, and then destained with the same fixing solution for 2 h.
- Silver stain: Gels were fixed for 5 min in a solution of 50% acetone, 1% TCA, and 0.015% formaldehyde. Gels were rinsed with diH2O for 5 s three times, followed by a 5-min rinse. After another quick rinse, gels were pretreated with 50% acetone for 5 min. Next, gels were treated with 0.02% sodium thiosulfate for 1 min, followed by three quick diH2O rinses. Gels were impregnated with 0.25% silver nitrate and 0.35% formaldehyde for 8 min, followed by two quick diH2O rinses. Bands were developed with a solution of 2% sodium carbonate, 0.015% formaldehyde, and 0.005% sodium thiosulfate for 15–20 min. Development was stopped by washing the gels with 1% glacial acetic acid for 30 s, followed by a 10-s rinse with diH2O.
- Zinc stain: Gels were briefly rinsed with diH2O and incubated in 0.2 M imidazole for 10 min. The gels were stained with 0.3 M zinc chloride for 30 s and then immediately rinsed with diH2O to prevent overstaining.
- Copper stain: Gels were briefly rinsed with diH2O, followed by 5 min of staining with 0.5 M copper chloride. The gels were then washed with diH2O for 3 min before imaging.
- Ponceau S: Gels were briefly rinsed with diH2O and stained for 5 min with Ponceau S. Destaining was performed with diH2O over 1 week, with multiple water changes. When destaining plateaued, the gels were submerged overnight in a solution of 50% methanol and 10% acetic acid, although this had a minimal effect.
- SYPRO Ruby: Gels were fixed for 30 min in a solution of 50% methanol and 7% acetic acid. This step was repeated with a fresh solution for another 30 min. Gels were stained overnight in the dark and then washed for 1 h with 10% methanol and 7% acetic acid, followed by two 5-min rinses with diH2O.
- SYPRO Orange, SYPRO Red, and SYPRO Tangerine: Stock solutions of SYPRO Orange, Red, and Tangerine were diluted 1:5000 in 7.5% acetic acid (Orange/Red) or diH2O (Tangerine). Gels were stained overnight in the dark. After staining, gels were briefly rinsed with either 7.5% acetic acid or diH2O, as appropriate.
- Coomassie Fluor Orange: Gels were stained overnight in the dark and then briefly rinsed with 7.5% acetic acid. Before imaging, gels were rinsed with diH2O for 5 min to decrease background intensity slightly.

In this study, we aimed to evaluate a broad range of polymers and staining combinations to identify the optimal platform for SDS-PAGE separation of proteins isolated using SMA and related polymers. The Bruce Lab maintains an extensive collection of polymers, comprising over 31 commercially available polymers [16] and more than 50 proprietary polymers developed by the Chemistry Department at the University of Tennessee, Knoxville (UTK) [17, 20, 37]. For this work, we focused exclusively on testing the commercially available polymers to ensure that our findings would be broadly applicable and beneficial to other researchers in the membrane protein field.

To maximize the number of polymers tested, we divided our experimental design into two subsets: one to evaluate polymers on thylakoid membranes and a separate subset on mitochondrial membranes. This approach allowed us to observe polymer-membrane interactions across different biological contexts, thereby enhancing the generalizability of our findings. For consistency and internal validation, we included one standard treatment, SMA 1440, in both membrane preparations. This provided a direct comparison between each polymer's performance with commonly used SDS-PAGE staining protocols.

In total, we tested 13 different polymers, assessing their compatibility with 15 various stains frequently used in protein electrophoresis. This comprehensive analysis enabled us to systematically compare the efficacy of polymers across stains, offering insights into which polymer-stain combinations are most effective for clear and reproducible protein band separation.

4 | Results

4.1 | Coomassie and Ponceau Staining of SMALPs

We conducted a comprehensive evaluation of various staining methods on thylakoid and mitochondrial membrane proteins solubilized using thirteen different SMA/DIBMA polymers to assess the protein detection sensitivity of each stain, polymer interference, and overall protein visualization quality (Figures 1 and 2). The thylakoid samples showed significant differences depending on the polymer used. SMA 1440 and DIBMA 12 produced a pronounced dark staining artifact across all molecular weight regions, consistent across all staining methods, and hindered clear visualization of protein bands. The BZ series only produces dark staining artifacts below ~10 kDa, making it preferable for high- and medium-molecular-weight proteins. Sulfo-based polymers uniquely exhibited no visible staining artifacts, even at low molecular weights. This is consistent with previous studies indicating that electroneutral Sulfo-based polymers bypass the electrophoretic obstruction characteristic of charged SMA and DIBMA polymers [38]. However, proteins captured by Sulfo-SMA and Sulfo-DIBMA also exhibited lower band intensity throughout

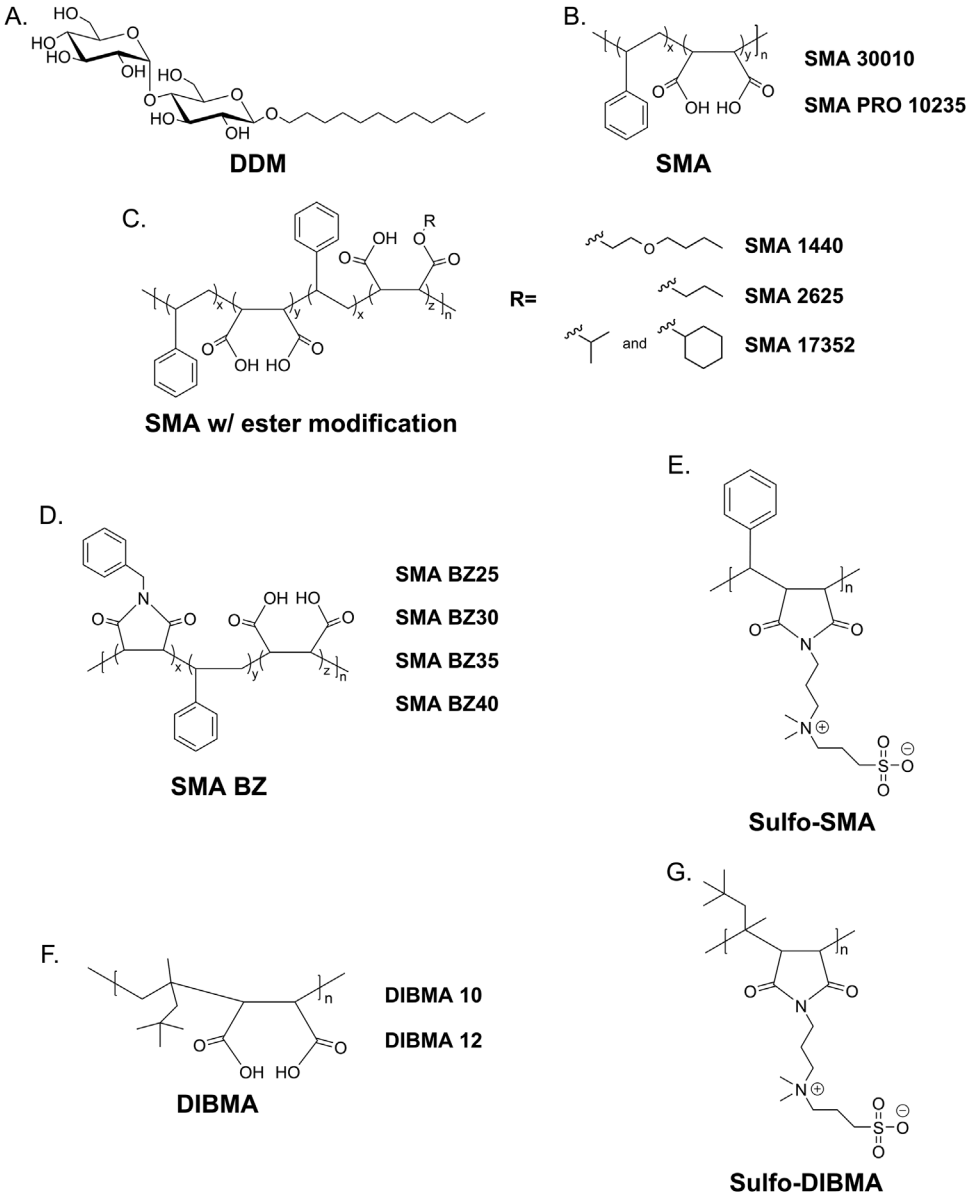

FIGURE 1 | Chemical structures of the detergent and copolymers used in this study. (A) n-Dodecyl-β-D-maltoside (DDM). (B) Unmodified styrenemaleic acid (SMA) copolymers: SMA 30010 and SMA Pro 10235. (C) Ester-modified maleic acid functionalities (three variants); the corresponding R-groups are indicated at right. (D) BZ-series SMA copolymers (poly(styrene-co-maleic acid-co-N-benzylmaleimide)); the numerical suffix denotes the mol% N-benzylmaleimide incorporated into the polymer chain. (E) Sulfo-SMA (poly(styrene-co-N',N'-dimethyl(maleimidoethyl)ammonium propane sulfonate)). (F) DIBMA copolymers; the numerical designation (10 or 12) indicates the alkyl chain length (C10 vs C12), with the C12 material having an average molecular weight of ˜12,000 and increased polymer hydrophobicity. (G) Sulfo-DIBMA, an electroneutral sulfonate-modified derivative of diisobutylenemaleic acid (DIBMA).

all molecular weight regions than proteins captured by all other polymers, indicating that Sulfo-based polymers isolate lower concentrations of membrane proteins than other polymers.

In mitochondrial membrane samples, DDM emerged as the least interfering solubilizing agent with minimal background interference across all stains. Still, it failed to extract a ~27 kDa protein, a limitation not observed in the polymers, except for DIBMA 10 (Figure 3). Among the SMA variants, SMA 2625 had the highest background interference, which complicated band detection. In contrast, SMA 1440 showed reduced interference compared to its performance with thylakoid samples, suggesting membrane composition-dependent variability. The BZ polymers, on the other hand, provided uniform band visualization in both thylakoid and mitochondrial membranes. GelCode Blue consistently outperformed other Coomassie stains, maintaining visibility despite the presence of polymer artifacts. Although Ponceau S minimized polymer interaction and reduced background noise in the 250 to ~20 kDa range, its lower sensitivity (Table 1) and incomplete destaining made it a less practical choice, especially for detecting low-abundance proteins.

Overall, GelCode Blue was the most effective staining method, offering high sensitivity and minimal polymer interference for a

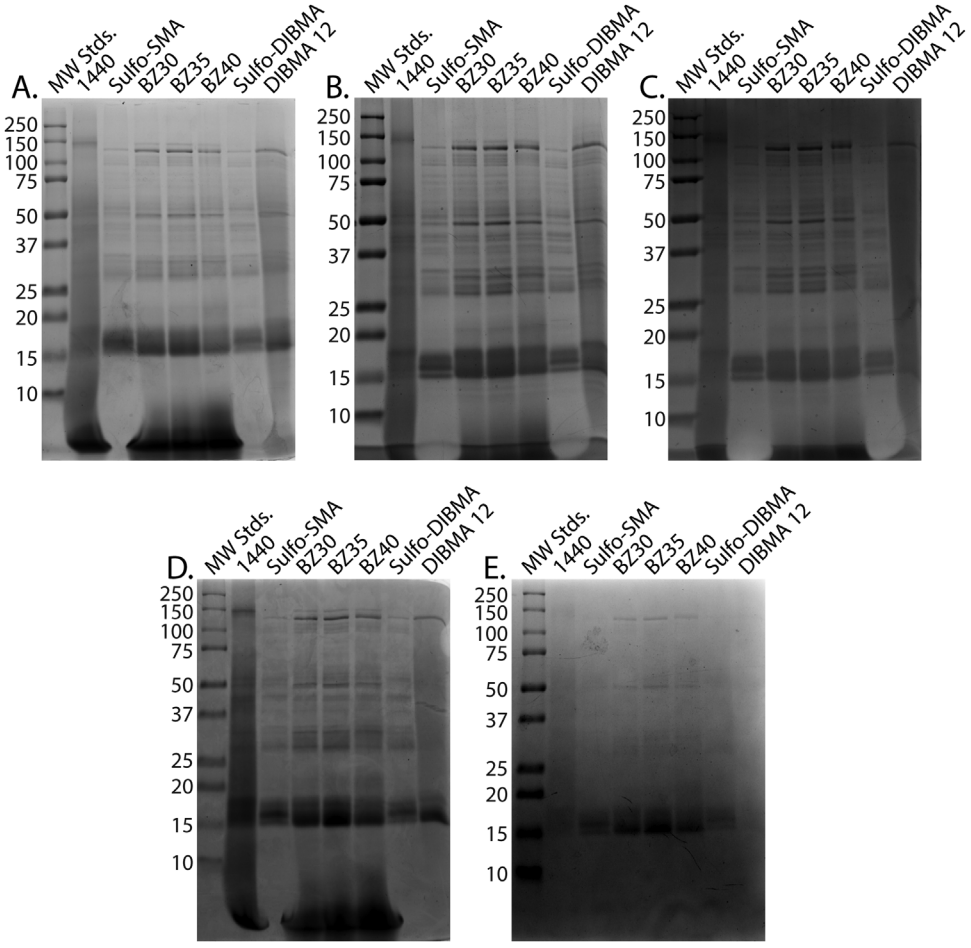

FIGURE 2 | SDS-PAGE visualization of solubilized cyanobacteria TS-821 thylakoid membrane proteins using various Coomassie Brilliant Blue stains and Ponceau S stain: (A) InstantBlue Coomassie, (B) GelCode Blue, (C) SimplyBlue SafeStain, (D) Coomassie R-250, and (E) Ponceau S. DIBMA, diisobutylene maleic acid; SMA, styrene-maleic acid.

TABLE 1 | Protein stain sensitivities: list of all protein stains used in this manuscript, arranged in ascending order of their staining sensitivities in nanograms of proteins.

Staining method	Sensitivity of protein detection (ng)
Silver stain	0.05–0.1
Zinc stain	0.25–0.5
SYPRO Ruby	1.0–2.0
SYPRO Orange	1.0–2.0
SYPRO Red	4.0–8.0
SYPRO Tangerine	4.0–8.0
InstantBlue Coomassie	5.00
SimplyBlue SafeStain	7.00
Coomassie Fluor Orange	8.00
GelCode Blue	9.00
Coomassie R-250	100.00
Ponceau S	200.00

broad range of protein sizes in both thylakoid and mitochondrial membranes. Its ability to bypass artifacts caused by polymer interactions makes it the optimal choice for diverse membrane solubilization protocols. InstantBlue Coomassie also bypassed polymer artifacts to a similar extent as GelCode Blue, but its lower sensitivity limits its application for low-abundance proteins. Coomassie R-250 was the least effective, offering low resolution without reducing background interference. Thus, GelCode Blue emerged as the most reliable and consistent staining method for SMA/DIBMA-solubilized membrane proteins, ensuring clear visualization across different experimental setups.

4.2 | Metal Staining of SMALPs

In addition to our evaluation of Coomassie and Ponceau stains, we tested metal stains—silver, zinc, and copper—on thylakoid and mitochondrial membrane samples following solubilization with SMA/DIBMA copolymers and DDM (Figures 4 and 5). These metal stains demonstrated different levels of sensitivity and protein visualization capability.

In the thylakoid samples (Figure 4 A–C), SMA 1440 and DIBMA 12 consistently produced high background levels, par-

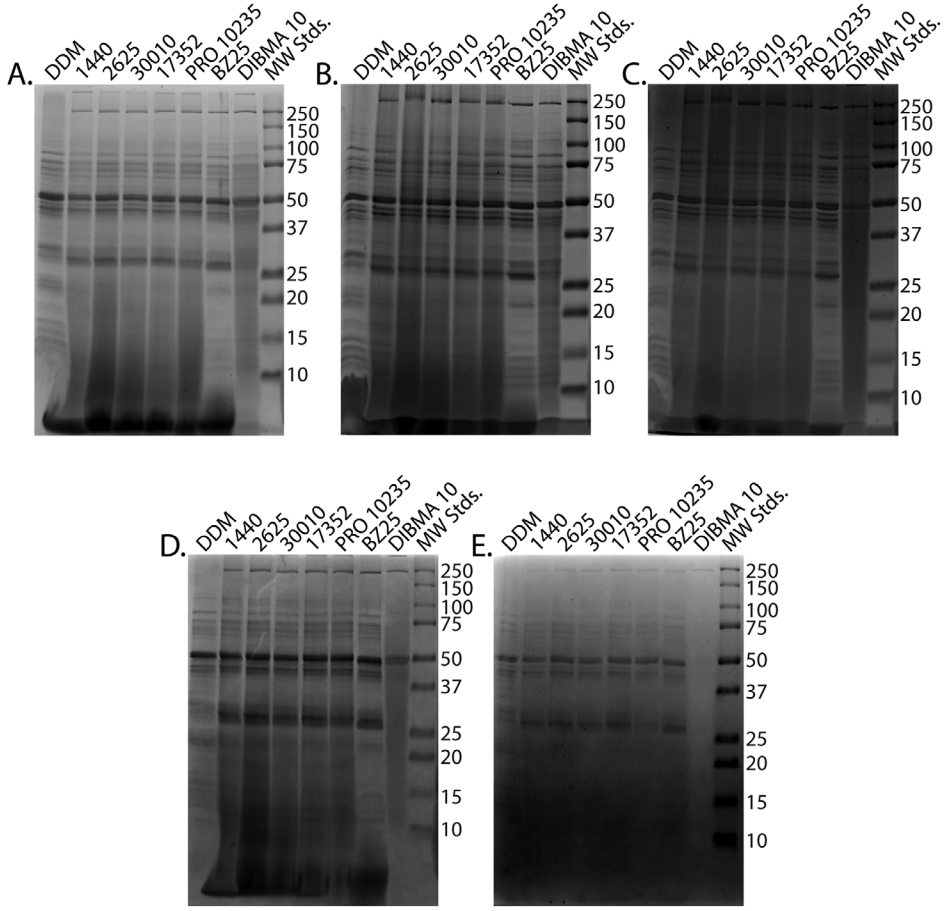

FIGURE 3 | SDS-PAGE visualization of solubilized bovine heart mitochondrial membrane proteins using various Coomassie Brilliant Blue stains and Ponceau S stain: (A) InstantBlue Coomassie, (B) GelCode Blue, (C) SimplyBlue SafeStain, (D) Coomassie R-250, and (E) Ponceau S. DDM, detergent *n*-dodecyl-*β*-D-maltoside; DIBMA, diisobutylene maleic acid.

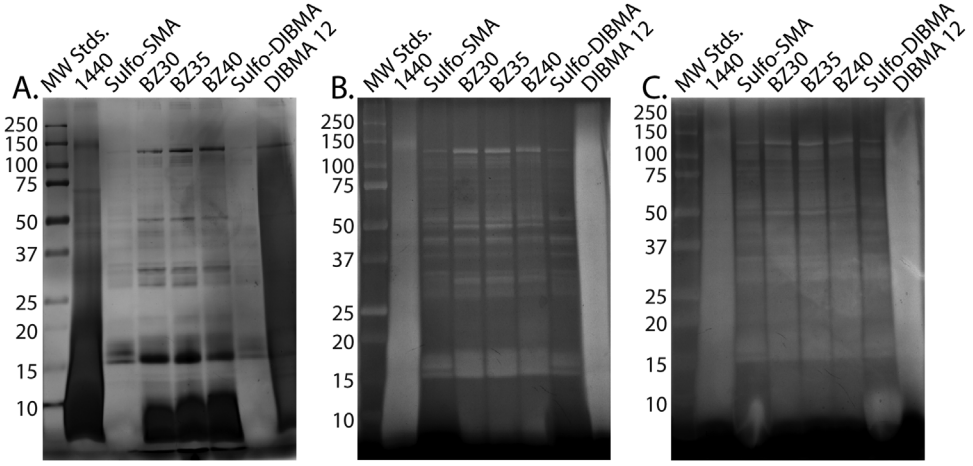

FIGURE 4 | SDS-PAGE visualization of solubilized cyanobacteria TS-821 thylakoid membrane proteins using various metal stains: (A) silver, (B) zinc, and (C) copper. DIBMA, diisobutylene maleic acid; SMA, styrene-maleic acid.

ticularly with copper staining (Figure 4C), where the entire lane was heavily obscured. DIBMA 12 performed the worst in this regard, showing background interference in the whole lane. However, Sulfo-SMA and Sulfo-DIBMA preferentially extracted lower molecular weight proteins (<20 kDa), better stained with zinc, providing high-intensity bands compared to the heavier proteins. The BZ polymers, particularly BZ30, BZ35, and BZ40, performed well across the metal stains, with zinc providing the best resolution and minimal background interference.

A similar trend was observed in the mitochondrial samples (Figure 5A–C). DIBMA 10 produced high background levels, reducing the clarity of the protein bands, with the highest background observed in SMA PRO 10235 across all three stains,

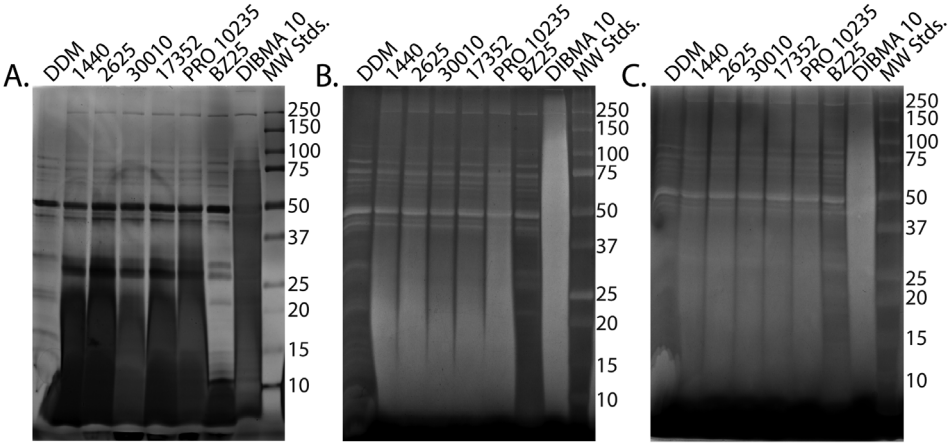

FIGURE 5 | SDS-PAGE visualization of solubilized bovine heart mitochondrial membrane proteins using various metal stains: (A) silver, (B) zinc, and (C) copper. DDM, detergent *n*-dodecyl-*β*-D-maltoside; DIBMA, diisobutylene maleic acid.

rather than in SMA 1440. BZ25 also had considerably lower polymer interference than all other polymers tested across all three stains, comparable to the performance of the other BZ polymers used with thylakoids. Across both membranes, copper staining consistently showed the lowest sensitivity for protein detection and the most polymer interference among the three stains. Zinc staining again provided the clearest visualization of higher molecular weight proteins (Figure 5B), outperforming silver and copper in sensitivity and resolution. However, the ~27 kDa protein in the silver stain was not visible due to background interference. Zinc staining emerged as the superior choice for both thylakoid and mitochondrial samples solubilized with SMA/DIBMA polymers, especially in reducing background and enhancing band resolution. However, zinc staining seemed to be most effective at minimizing the background of membrane samples solubilized by polymers that already had low interference, such as the BZ series and Sulfo-based polymers. When staining samples solubilized by polymers of higher interference, it seemed to increase background staining, as evidenced by SMA 1440, 2625, 30010, and PRO 10235. Thus, silver staining (Figure 5A) may be a preferable alternative when using these polymers, as it produced clearer band resolution for these samples despite having a higher background signal.

4.3 | Fluorescent Staining of SMALPs

In addition to testing traditional stains like Coomassie, Ponceau S, and metal-based stains, we evaluated the performance of various fluorescent stains—SYPRO Ruby, SYPRO Orange, SYPRO Red, SYPRO Tangerine, and Coomassie Fluor Orange—on thylakoid and mitochondrial membrane samples (Figures 6 and 7). Although all these fluorescent stains demonstrated comparable performance, subtle differences in band visibility and background interference were observed. In the thylakoid samples (Figure 6A–E), SYPRO Ruby stood out with the highest band resolution among the tested stains (Figure 6A). However, SYPRO Orange uniquely detected proteins below 20 kDa, which was not achieved by other stains, such as SYPRO Red and SYPRO Tangerine. Although SYPRO Red and SYPRO Tangerine exhibited lower background interference, they also showed a reduced ability to detect proteins, suggesting limited sensitivity. Coomassie Fluor Orange performed similarly to SYPRO Ruby and Orange. Still, it demonstrated lower resolution and failed to detect low-molecular-weight proteins, highlighting SYPRO Orange as the superior option for resolving smaller proteins.

Similar staining patterns were noted for mitochondrial membrane samples (Figure 7A–E). DIBMA 10 showed the highest background staining among all DIBMA variants, whereas SMA 2625 and SMA PRO 10235 produced significant background interference among the SMA polymers. However, the BZ25 variant displayed exceptional protein band clarity with minimal polymer interference, confirming its reliability across different staining techniques. Interestingly, Sulfo-SMA and Sulfo-DIBMA, which previously exhibited weak protein staining, showed even lower protein detection with fluorescent stains than other methods, further underscoring the challenges associated with specific polymer variants.

Overall, SYPRO Ruby emerged as the most effective fluorescent stain for thylakoid and mitochondrial membrane samples (Figure 7A), producing sharp band resolution and low background interference. SYPRO Orange also proved valuable, particularly for detecting low-molecular-weight proteins, making it a strong alternative when small protein fragments are of interest. Although differences between the fluorescent stains were minimal, the choice of stain should be tailored to the sample's specific molecular weight range and background properties, with SYPRO Ruby being the optimal choice for overall clarity and SYPRO Orange offering unique benefits for visualizing proteins with lower molecular weights.

4.4 | Stain-Free Visualization of SMALPs

The final method we examined for visualizing SMALPs was stain-free imaging using TCE incorporated directly into the gel to form fluorophores bound to proteins. We compared commercially available precast stain-free gels with manually cast TCE gels using our thylakoid and mitochondrial membrane samples (Figures 8 and 9). Each approach yielded distinct differences in resolution and background interference.

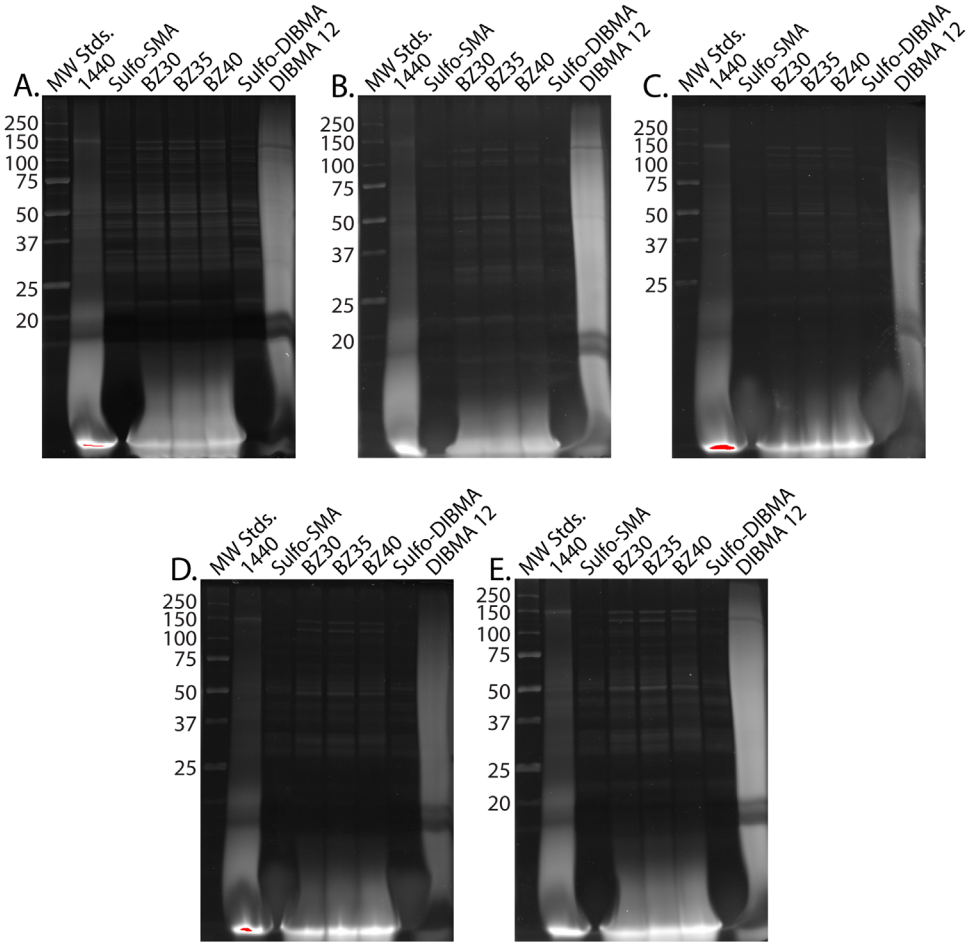

FIGURE 6 | SDS-PAGE visualization of solubilized cyanobacteria TS-821 thylakoid membrane proteins using various fluorescent stains: (A) SYPRO Ruby, (B) SYPRO Orange, (C) SYPRO Red, (D) SYPRO Tangerine, (E) Coomassie Fluor Orange. DIBMA, diisobutylene maleic acid; SMA, styrene-maleic acid.

For thylakoid samples (Figure 8A,B), SMA 1440 exhibited the highest background interference among the polymers tested across both stain-free gel types. In contrast, DIBMA 12 showed minimal background staining, outperforming all previously used methods. Additionally, in the manually cast TCE gel (Figure 8B), the BZ series did not display the typical dark staining artifact below 10 kDa that we observed with other techniques. Despite the interference observed in the SMA 1440 lane, stain-free visualization resulted in substantially reduced background staining for all polymers compared to earlier staining methods. Notably, the manually cast TCE gel demonstrated both lower polymer interference and sharper band resolution compared to the Any kD Mini-PROTEAN TGX Precast Protein Gel (Figure 8A). Although the exact polyacrylamide gradient of the precast gel is unspecified, its limited ability to visualize proteins below 15 kDa suggests a lower maximum acrylamide density than the 10%–20% gradient used in our TCE gels.

Consequently, the TGX Precast Gel could not confirm whether the dark staining artifact below 10 kDa in the BZ series was still present. In contrast, the TCE gel showed that this artifact was eliminated and significantly reduced the background staining in the SMA 1440 lane compared to the precast gel. Overall, the manually cast TCE gel provided enhanced sensitivity and resolution, producing sharper bands than the precast option.

The benefits of the TCE gel were even more pronounced with mitochondrial membrane samples (Figure 9A,B), where the reductions in background interference and improvements in resolution were more evident. Background staining was minimal for all polymers tested, particularly in the manually cast TCE gel (Figure 9B). Although SMA 2625 produced minor polymer interference, it was low enough to be considered negligible. Even DIBMA 10 showed no visible background staining, achieving a resolution comparable to that of SMA polymers and DDM—a result that no previous staining method had achieved. Ultimately, the manually cast TCE gel emerged as the superior technique for protein visualization due to its significantly higher sensitivity and resolution than Any kD Mini-PROTEAN TGX Precast Protein Gels (Figure 9A). Although other precast gels with different acrylamide densities and gradients might yield better results, the flexibility and customizability of manually cast gels make them more versatile and easier to optimize for specific experimental conditions. Compared to all previously studied techniques, the clear resolution and minimal background interference achieved with TCE gels establish them as the preferred method for analyzing SMA/DIBMA-solubilized samples via SDS-PAGE.

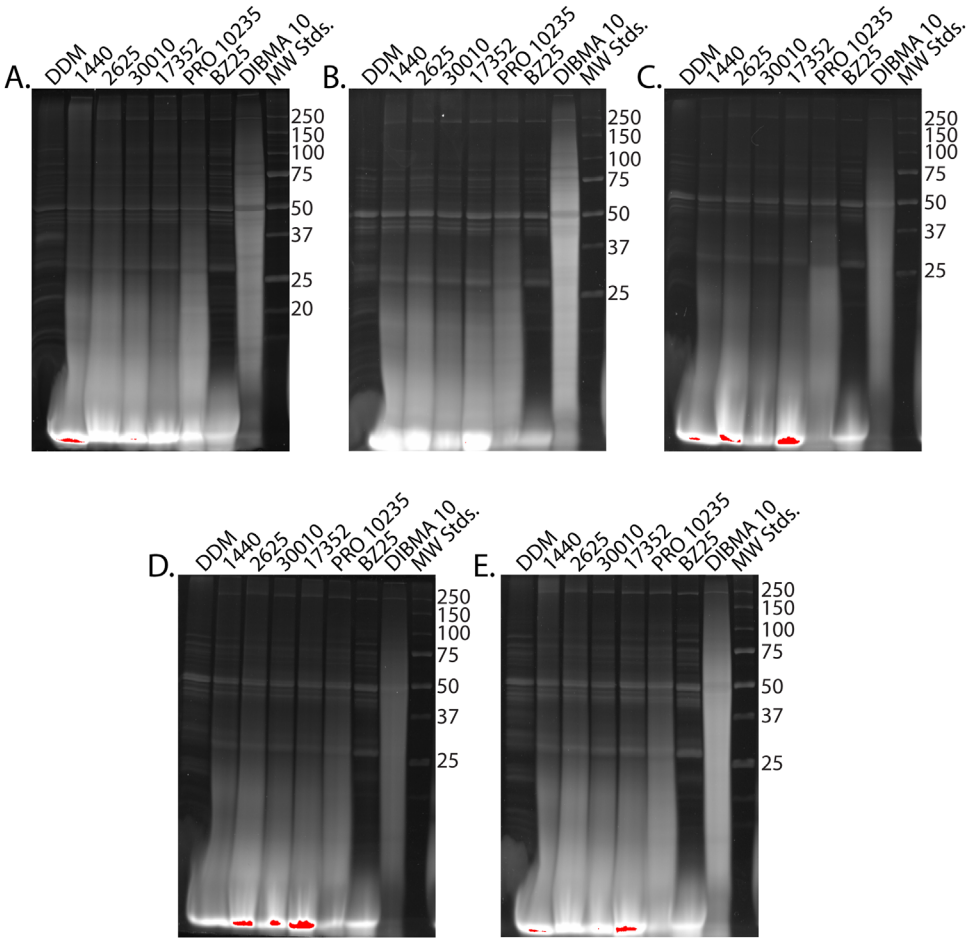

FIGURE 7 | SDS-PAGE visualization of solubilized bovine heart mitochondrial membrane proteins using various fluorescent stains: (A) SYPRO Ruby, (B) SYPRO Orange, (C) SYPRO Red, (D) SYPRO Tangerine, (E) Coomassie Fluor Orange. DDM, detergent *n*-dodecyl-*β*-D-maltoside; DIBMA, diisobutylene maleic acid.

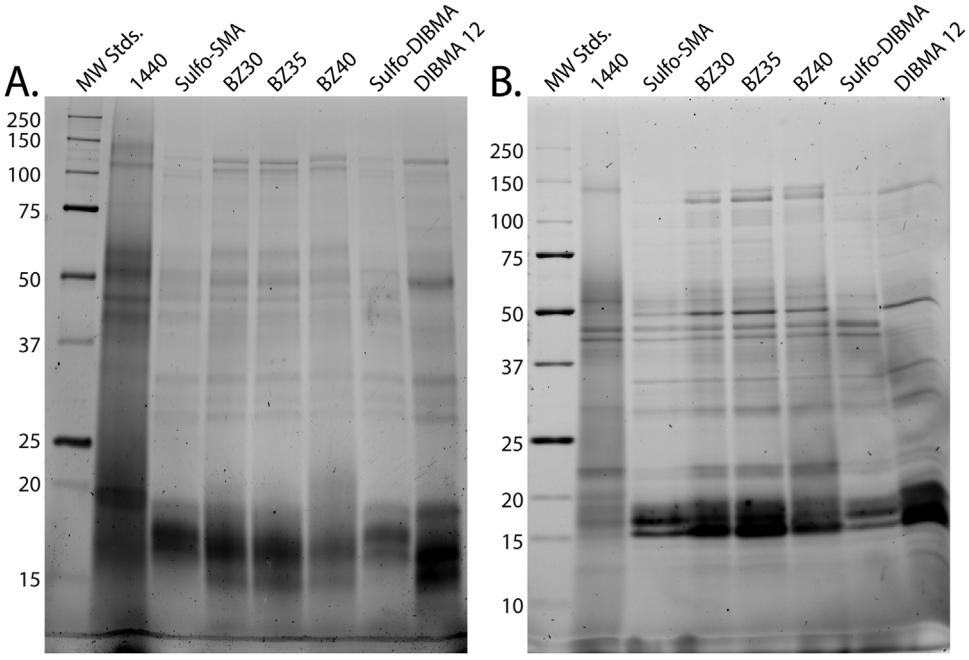

FIGURE 8 | SDS-PAGE visualization of solubilized cyanobacteria TS-821 thylakoid membrane proteins using stain-free UV photoactivation: (A) Any kD Mini-PROTEAN TGX Precast Protein Gels (Bio-Rad), (B) in-house made 12%–20% gradient gel with 0.5 % TCE final concentration in acrylamide as visualized after UV photoactivation. DIBMA, diisobutylene maleic acid.

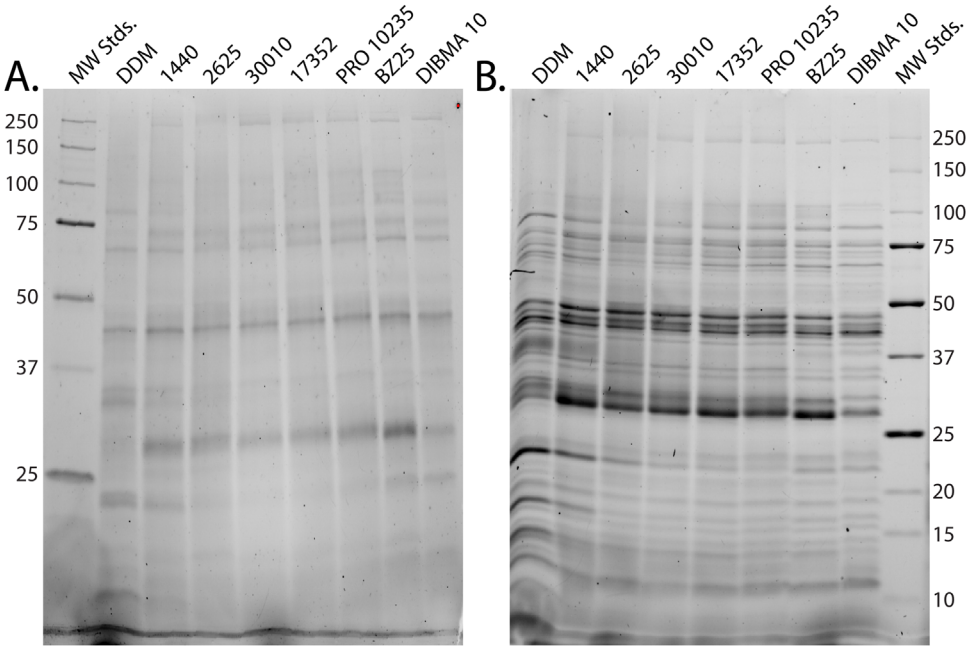

FIGURE 9 | SDS-PAGE visualization of solubilized bovine heart mitochondrial membrane proteins using stain-free UV photoactivation: (A) Any kD Mini-PROTEAN TGX Precast Protein Gels (Bio-Rad), (B) in-house made 12%–20% gradient gel with 0.5 % TCE final concentration in acrylamide as visualized after UV photoactivation. DDM, detergent *n*-dodecyl-*β*-D-maltoside; DIBMA, diisobutylene maleic acid.

4.5 | Visualization of Native SMALP Complexes Using TCE in CN-PAGE

We evaluated whether TCE could stain membrane proteins that remain in their native state within SMALPs, thereby testing its ability to penetrate the lipid–polymer annulus and react with aromatic residues likely buried within the hydrophobic core. Thylakoid membrane protein complexes were solubilized using DDM or one of three copolymers—SMA 30010, BZ35, and BZ40—and separated by CN-PAGE with TCE incorporated directly into the resolving gel (Figure 10A). In all cases, a distinct fluorescent band was observed at an apparent molecular weight of approximately 500 kDa, indicating that TCE can effectively label large native membrane assemblies within both polymer- and detergent-solubilized samples.

Subsequent staining of the same gels with colloidal CBB produced a nearly identical banding pattern (Figure 10B), confirming that TCE-based stain-free detection is compatible with standard post-staining visualization and provides comparable sensitivity and resolution. We further extended this staining method to SMALPs separated using native electrophoresis, demonstrating that TCE can be applied broadly for visualizing native membrane complexes across different gel systems. These results establish TCE as an effective, low-cost reagent for imaging native membrane–protein complexes resolved by CN-PAGE and related electrophoretic methods.

In contrast, when proteins were separated by BN-PAGE, the in-gel binding of Coomassie G-250 appeared to quench the TCE fluorescence, substantially reducing detectability (data not shown). This finding underscores the need to optimize gel and staining conditions when applying TCE-based detection to native protein complexes.

4.6 | Qualitative Ranking of Staining Methods

To systematically assess the effectiveness of various staining methods used throughout Figures 2–9, we conducted a blind, qualitative evaluation with input from multiple independent observers. Our evaluation panel consisted of seven undergraduate and graduate students from diverse biological disciplines, providing a range of perspectives on membrane protein visualization. Each observer rated individual gel lanes for background intensity and band clarity using a scale from −5 (lowest) to +5 (highest). These ratings were compiled and transformed into a comprehensive heatmap to represent the results visually (Figure 11).

The resulting heatmap provided clear insights into the relative performance of each staining technique across both mitochondrial and thylakoid membrane proteins solubilized by various polymers. DIBMA 10 was consistently ranked as the least effective staining method for mitochondrial proteins, with poor band visualization and elevated background interference. However, when these proteins were visualized using our custom in-house stain-free gel, the clarity of the protein bands improved dramatically, surpassing even the commonly used GelCode Blue in terms of sensitivity and resolution. This significant enhancement highlights the effectiveness of our stain-free method in overcoming the limitations typically associated with DIBMA solubilization.

Similarly, for thylakoid membrane samples, SMA 1440 and DIBMA 12 both exhibited suboptimal staining across nearly all traditional methods, resulting in faint bands and high background. Remarkably, band resolution improved substantially when these samples were visualized using our TCE-based stain-free gel, providing clear and distinct protein bands with

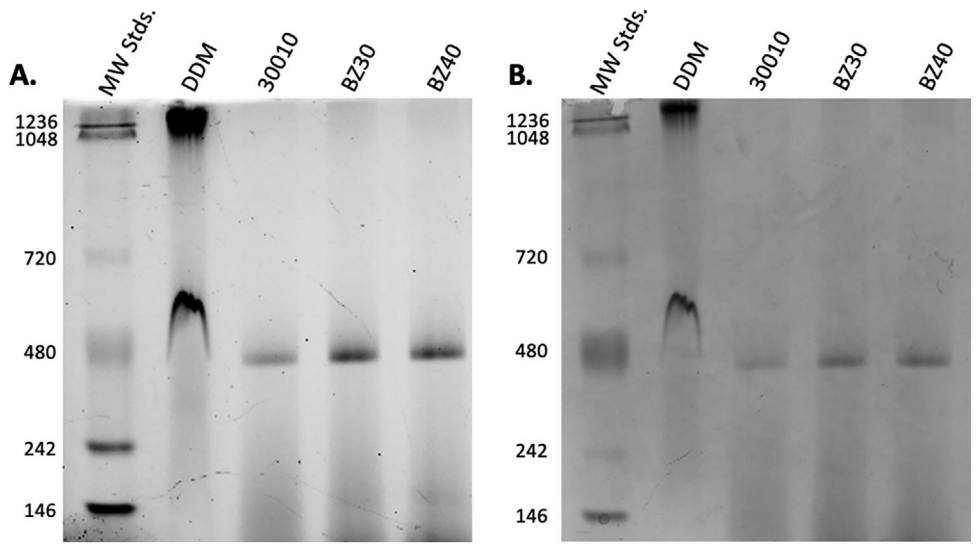

FIGURE 10 | CN-PAGE visualization of solubilized chloroplast membrane proteins: (A) fluorescent image of in-house 3%–8% acrylamide gradient gel with TCE (0.5% final concentration) visualized after UV photoactivation, (B) white light imaging of the same in-house gel in A visualized after overnight staining with InstantBlue colloidal Coomassie staining.

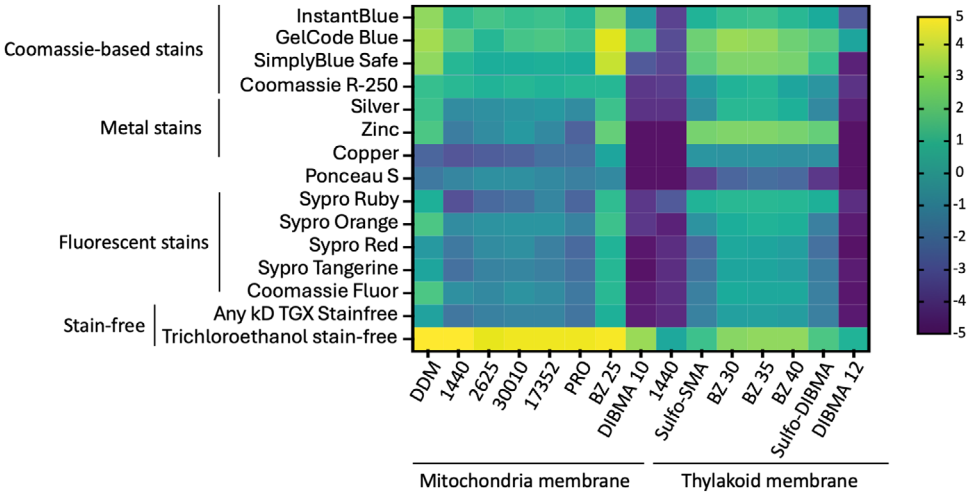

FIGURE 11 | Qualitative rating of staining method performance: compilation of the stain performance and polymer solubilization capability of membrane proteins. The final cell value is based on the average blind score given to the observed background level for all the gels. Stains are arranged according to their type (or family) on the vertical axis, and solubilized samples are on the horizontal axis, where they are segregated into two groups based on their origin. The scale on the right shows the lowest (−5) and highest (5) possible scores and the corresponding color gradient. This was based on the average of seven independent "observers" invited to rank the multiple samples on different stained gels. DDM, detergent *n*-dodecyl-*β*-D-maltoside; DIBMA, diisobutylene maleic acid; SMA, styrene-maleic acid.

minimal background interference. These findings demonstrate the reliability and robustness of our custom stain-free method for accurately resolving protein bands, even in samples where conventional staining methods failed.

Furthermore, the heatmap revealed that standard stains, such as copper and SYPRO Ruby, were less effective for mitochondrial samples, yielding inconsistent band patterns and increased noise. Ponceau S, a commonly used stain for membrane proteins, struggled to provide adequate staining for solubilized thylakoid membrane proteins, resulting in a lack of detectable bands. In contrast, our stain-free method consistently outperformed all other techniques tested, demonstrating compatibility with nearly every polymer and sample type. This consistent success suggests that TCE interacts uniquely with protein residues, forming fluorophores that are less affected by the presence of solubilizing agents. This characteristic likely explains why our stain-free method yields high-resolution protein bands, whereas other methods are hindered by polymer interference.

4.7 | Principle and Mechanism of TCE-Based Fluorescent Labeling

Proteins resolved by SDS-PAGE or CN-PAGE can be rapidly visualized by soaking gels in 2,2,2-TCE and illuminating with

UV light. The UV-driven reaction of tryptophan with trichloro compounds yields fluorescent products in the visible range, revealing protein bands [39]. Upon UV exposure, TCE reacts with tryptophan and tyrosine residues, forming covalently modified species with red-shifted fluorescence [36, 40, 41]. Although native tryptophan fluoresces at ~350 nm, this emission is weak in aqueous solution. UV-induced photochemical modification acylates the indole ring, shifting the fluorescence to wavelengths above 450 nm. Tyrosine also undergoes photochemical labeling via distinct mechanisms [37]. TCE can be incorporated during gel casting or added post-electrophoresis in solution to enable rapid UV-induced visualization. Although other trichlorinated compounds, such as TCA and chloroform, exhibit similar properties, TCE delivers superior performance when precast in gels [37].

TCE visualization appears broadly compatible with downstream proteomics. Prior work by Ladner et al.,[40] identified TCE-visualized proteins from 2D gels by both MALDI-TOF peptide mass fingerprinting and LC–MS/MS, noting that the UV-driven adduct forms at low stoichiometry predominantly on tryptophan and that confident identifications were obtained without specifying a Trp modification during database searching. Mechanistically, the photoadduct imparts an optional diagnostic mass shift of ~+58 Da on Trp; thus, when desired, searches can be performed with and without a variable +58 Da on W (allowing one missed cleavage) to assess the neutrality of the visualization step and to localize modified sites. Given the sensitivity of current high-resolution instruments and search engines, we anticipate equal or improved peptide and protein IDs relative to earlier reports. Although we did not perform MS on TCE-visualized bands here (from SDS-PAGE or CN-PAGE), future work will explicitly benchmark identification rates and site localization in our system and explore whether low-stoichiometry Trp adduction can serve as a coarse probe of residue accessibility in membrane proteins.

4.8 | Development of a Fluorescence Assay for Surface-Accessible Residues

Building on established principles, we developed a protein quantification assay using TCE-mediated fluorescence. Proteins in solution were treated with 1% TCE and exposed to near-UV light, resulting in strong, quantifiable fluorescence with an emission maximum at approximately 463–468 nm upon excitation at 310 nm. This method relies on covalent photochemical labeling of solvent-accessible tryptophan and tyrosine residues, resulting in a robust and reproducible signal suitable for high-throughput microplate analysis. UV activation of TCE forms reactive species that selectively modify exposed aromatic residues, while buried sites remain unreactive. This fluorescence enhancement enables both visualization and quantification of protein content, offering a tool for assessing conformational states. Additionally, this reagent does not interact with any of the 12 different free polymers that migrate ahead of proteins in the Laemmli gel system, significantly improving the visibility of solubilized proteins. Interestingly, upon UV exposure, we observe two fluorescence peaks: one near 460 nm and a small shoulder at ~490 nm, potentially corresponding to TCE interactions with tyrosine and tryptophan, respectively (Figure 12A,B).

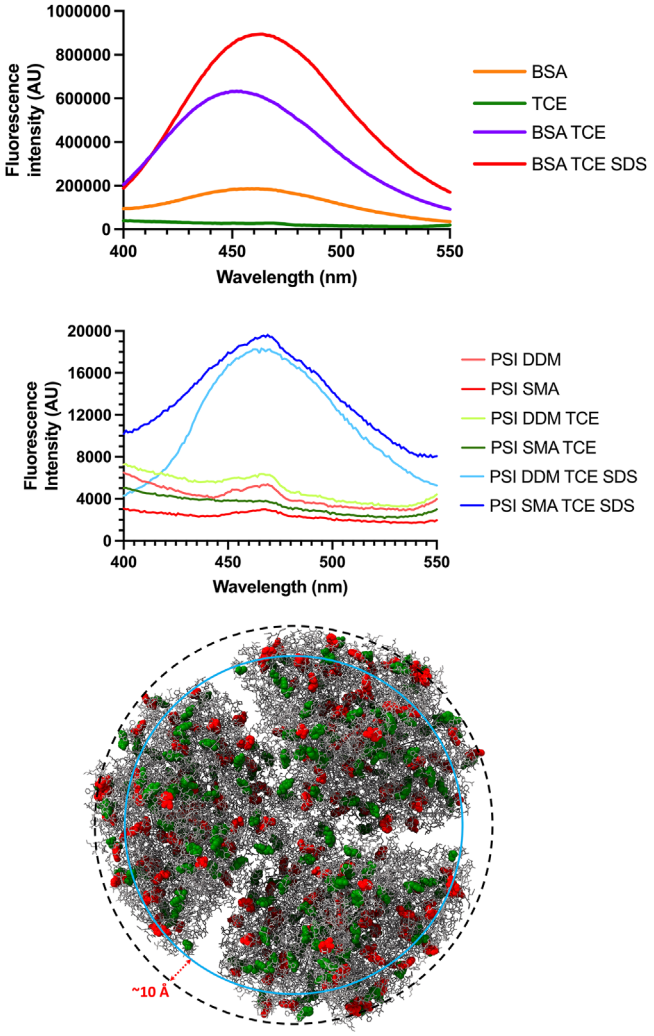

FIGURE 12 | TCE photoactivation enhances protein fluorescence in both membrane and non-membrane proteins: (A) Fluorescence intensities of samples after exposure to UV. BSA and TCE do not have significant fluorescence, but the BSA-TCE mixture has significant fluorescence after exposure to UV, which is further enhanced after protein melting using SDS. Ratio of area under the curve (AUC) for BSA TCE SDS: BSA TCE is 1.64. (B) Similarly, cyanobacterial photosystem I (PSI) solubilized using detergent and non-detergent methods has negligible fluorescence, but after mixing with TCE, fluorescence is increased considerably. Protein denaturation using SDS substantially increases fluorescence, which is correlated to the number of buried Tyr and Trp residues in the folded PSI structure. (C) Native PSI structure displays only a limited number of tryptophan and tyrosine residues accessible at the surface, highlighted as red and green, respectively. But all aromatic residues can be exposed by denaturing PSI, an approximate tenfold increase. The inner circle indicates an approximate distance of 10 Å from the edge. BSA, bovine serum albumin; DDM, detergent *n*-dodecyl-*β*-D-maltoside; PSI, photosystem I; SMA, styrene-maleic acid; TCE, trichloroethanol.

As a proof-of-principle validation of our photo-crosslinking strategy, we applied TCE to BSA, a well-characterized small globular protein containing 20 tyrosine and 2 tryptophan residues. In its native state, BSA and TCE by themselves exhibited no appreciable fluorescence. However, after the addition of TCE to BSA, followed by UV photoactivation, the fluorescence intensity was significantly enhanced. Finally, to probe if the surface availability of

tyrosines or tryptophans would modulate fluorescence intensity, we treated the BSA-TCE mixture with a denaturing level of SDS. Denatured BSA had a 64% higher area under the curve (AUC) compared to BSA in its native form. This change can be attributed to the unfolding of the BSA tertiary structure, exposing buried tyrosines and tryptophans to TCE. These findings support our hypothesis that surface available residues interact with TCE and that surface availability can lead to higher fluorescence intensity, establishing TCE as a sensitive reporter for side chain accessibility (Figure 11A).

To further evaluate this labeling strategy with a complex membrane protein, we studied the cyanobacterial PSI trimer, a ~1 MDa multisubunit complex comprising 13 distinct subunits from *Thermosynechococcus elongatus* (now known as *Thermosynechococcus vestitus*). PSI was isolated by solubilizing using detergent DDM (PSI DDM) and polymer SMA 1440 (PSI SMA). Polymer extraction preserves ~800 native lipids in a detergent-free, nanodisc-like structure. When the intact native PSI complex was stained with TCE and irradiated with UV light, we observed modest fluorescence with an emission peak at approximately 463 nm (Figure 11B). This limited signal is consistent with the restricted accessibility of aromatic residues in the folded protein state. Following denaturation with SDS and heat treatment, fluorescence intensity at 425 nm increased several-fold (Figure 11B). Analysis of the published x-ray diffraction structure (PDB 1JB0) shows 27 tryptophan and 30 tyrosine residues within 10 Å of the protein surface in the native trimer [42], increasing to approximately 450 residues upon complete denaturation. These newly exposed residues (219 Trp and 231 Tyr, in total) are readily labeled by TCE, explaining the observed fluorescence increase.

As shown in Figure 12C, the native PSI structure displays only a limited number of tryptophan and tyrosine residues accessible on the surface, highlighted as red and green space-filling models. In contrast, Figure 12C visualizes all aromatic residues exposed in the denatured form, demonstrating an approximate eightfold increase in accessible sites. Interestingly, when we performed the same assay on a DDM-solubilized PSI preparation, the fluorescence at 425 nm was only slightly higher than that of the native SMA-solubilized form. This suggests that the polymer belt of SMA 1440 may only slightly occlude or restrict access of TCE to surface-exposed aromatic residues. Alternatively, this could indicate that PSI undergoes a partial or local unfolding upon solubilization in a DDM detergent micelle, which exposes additional Trp or Tyr residues. Finally, the SMA-solubilized PSI preparation has higher net fluorescence after denaturation, suggesting that this method might preserve additional amino acid residues compared to detergent-solubilized PSI.

5 | Conclusions

In conclusion, our customized stain-free method proved to be the most versatile and effective staining technique for various SMA/DIBMA-solubilized membrane proteins. The method's independence from polymer interference and its ability to enhance protein band resolution make it a powerful tool for researchers dealing with challenging solubilization agents. Its success in mitochondrial and thylakoid membrane samples underscores its potential as a universal staining solution. Implementing this approach in future studies will provide researchers with a reliable and reproducible method for protein visualization, helping to overcome common challenges associated with SMA and DIBMA solubilization.

The insights gained from this study have significant implications beyond the immediate context of SMA and DIBMA copolymer solubilization and SDS-PAGE analysis. The ability to effectively isolate and visualize low molecular weight subunits of membrane proteins is crucial for a wide range of biochemical and structural studies. The methods and findings from our research can be extended to other areas of membrane protein isolation and characterization where the accurate analysis of small subunits is essential.

One of the most attractive features of the stain-free protein detection technique we evaluated is its high sensitivity, enabling the detection of proteins at submicrogram levels. This method is also rapid and largely non-denaturing, making it ideal for preserving protein integrity during analysis. The stain-free approach can also be integrated into other assays, such as isoelectric focusing, sucrose density gradient centrifugation, and column chromatography, providing a versatile tool for comprehensive protein characterization. These features make it particularly useful for studying membrane proteins, where maintaining native conformations and interactions is critical.

However, one limitation of this stain-free method is its reliance on proteins rich in tryptophan residues, which may restrict its applicability to specific proteins. Fortunately, this is not typically a problem for most membrane proteins, as they generally contain sufficient tryptophan residues to be effectively detected using this technique. This makes the stain-free approach a valuable addition to the toolkit for membrane protein research, particularly in applications that require the detection and analysis of low-molecular-weight subunits.

As demonstrated in this study, the ability to minimize background interference in SDS-PAGE is particularly valuable for analyzing complex proteomes, such as those found in microbial membranes or specialized tissues like the brain or heart. Low-molecular-weight proteins often perform key regulatory or structural functions in these systems, and their accurate identification and quantification are crucial for understanding the broader biological processes at play. Our developed approaches can be adapted to isolate and study these proteins, providing a clearer understanding of their roles in membrane-associated functions. Furthermore, our results also demonstrate that UV-activated TCE-mediated fluorescence intensity scales directly with the surface-exposed population of tyrosine and tryptophan residues, thus providing a sensitive readout of protein conformation and residue accessibility.

Additionally, this work can be applied to the development of novel therapeutics targeting membrane proteins. Many drug targets are membrane-bound proteins, including G protein-coupled receptors (GPCRs), ion channels, and transporters. The ability to isolate and study these proteins with their associated lipids intact, especially those with low-molecular-weight subunits, can lead to a better understanding of their structure-function relationships, ultimately aiding in the design of more effective drugs.

In conclusion, the methodologies and findings presented in this study offer a robust framework for extending membrane protein research into new and challenging areas. By facilitating the isolation and accurate characterization of low-molecular-weight subunits, these techniques can significantly advance our understanding of membrane protein function in various biological contexts, paving the way for discoveries and applications in biochemistry, cell biology, and drug development.

Conflicts of Interest

The authors declare no conflicts of interest.

Data Availability Statement

Data sharing not applicable to this article as no datasets were generated or analyzed during the current study.

References

1. D. Lichtenberg, R. J. Robson, and E. A. Dennis, "Solubilization of Phospholipids by Detergents. Structural and Kinetic Aspects," *Biochimica Et Biophysica Acta* 737 (1983): 285–304, https://doi.org/10.1016/0304-4157(83)90004-7.

2. M. N. Jones, "Surfactants in Membrane Solubilisation," *International Journal of Pharmaceutics* 177 (1999): 137–159, https://doi.org/10.1016/s0378-5173(98)00345-7.

3. D. Linke, "Detergents: An Overview," *Methods in Enzymology* 463 (2009): 603–617, https://doi.org/10.1016/S0076-6879(09)63034-2.

4. G. Ratkeviciute, B. F. Cooper, and T. J. Knowles, "Methods for the Solubilisation of Membrane Proteins: The Micelle-Aneous World of Membrane Protein Solubilisation," *Biochemical Society Transactions* 49 (2021): 1763–1777, https://doi.org/10.1042/BST20210181.

5. A. M. Seddon, P. Curnow, and P. J. Booth, "Membrane Proteins, Lipids and Detergents: Not Just a Soap Opera," *Biochimica Et Biophysica Acta* 1666 (2004): 105–117, https://doi.org/10.1016/j.bbamem.2004.04.011.

6. A. G. Lee, "Lipid-Protein Interactions in Biological Membranes: A Structural Perspective," *Biochimica Et Biophysica Acta* 1612 (2003): 1–40, https://doi.org/10.1016/s0005-2736(03)00056-7.

7. S. Majeed, A. B. Ahmad, U. Sehar, and E. R. Georgieva, "Lipid Membrane Mimetics in Functional and Structural Studies of Integral Membrane Proteins," *Membranes (Basel)* 11 (2021): 685, https://doi.org/10.3390/membranes11090685.

8. H. X. Zhou and T. A. Cross, "Influences of Membrane Mimetic Environments on Membrane Protein Structures," *Annual Review of Biophysics* 42 (2013): 361–392, https://doi.org/10.1146/annurev-biophys-083012-130326.

9. S. C. Lee and N. L. Pollock, "Membrane Proteins: Is the Future Disc Shaped?," *Biochemical Society Transactions* 44 (2016): 1011–1018, https://doi.org/10.1042/BST20160015.

10. D. Hardy, R. M. Bill, A. Jawhari, and A. J. Rothnie, "Overcoming Bottlenecks in the Membrane Protein Structural Biology Pipeline," *Biochemical Society Transactions* 44 (2016): 838–844, https://doi.org/10.1042/BST20160049.

11. J. M. Dorr, S. Scheidelaar, M. C. Koorengevel, et al., "The Styrene-Maleic Acid Copolymer: A Versatile Tool in Membrane Research," *European Biophysics Journal* 45 (2016): 3–21, https://doi.org/10.1007/s00249-015-1093-y.

12. O. Korotych, J. Mondal, K. M. Gattás-Asfura, J. Hendricks, and B. D. Bruce, "Evaluation of Commercially Available Styrene-Co-Maleic Acid Polymers for the Extraction of Membrane Proteins From Spinach Chloroplast Thylakoids," *European Polymer Journal* 114 (2019): 485–500, https://doi.org/10.1016/j.eurpolymj.2018.10.035.

13. C. E. Workman, P. Bag, B. Cawthon, et al., "Alternatives to Styrene- and Diisobutylene-Based Copolymers for Membrane Protein Solubilization via Nanodisc Formation," *Angewandte Chemie International Edition* 62 (2023): e202306572, https://doi.org/10.1002/anie.202306572.

14. N. G. Brady, S. Qian, J. Nguyen, H. M. O'Neill, and B. D. Bruce, "Small Angle Neutron Scattering and Lipidomic Analysis of a Native, Trimeric PSI-SMALP From a Thermophilic Cyanobacteria," *Biochimica Et Biophysica Acta (BBA)—Bioenergetics* 1863 (2022): 148596, https://doi.org/10.1016/j.bbabio.2022.148596.

15. O. I. Korotych, T. T. Nguyen, B. C. Reagan, T. M. Burch-Smith, and B. D. Bruce, "Poly(Styrene-Co-Maleic Acid)-Mediated Isolation of Supramolecular Membrane Protein Complexes From Plant Thylakoids," *Biochimica Et Biophysica Acta (BBA)—Bioenergetics* 1862 (2021): 148347, https://doi.org/10.1016/j.bbabio.2020.148347.

16. N. G. Brady, C. E. Workman, B. Cawthon, B. D. Bruce, and B. K. Long, "Protein Extraction Efficiency and Selectivity of Esterified Styrene-Maleic Acid Copolymers in Thylakoid Membranes," *Biomacromolecules* 22 (2021): 2544–2553, https://doi.org/10.1021/acs.biomac.1c00274.

17. T. J. Knowles, R. Finka, C. Smith, Y. P. Lin, T. Dafforn, and M. Overduin, "Membrane Proteins Solubilized Intact in Lipid Containing Nanoparticles Bounded by Styrene Maleic Acid Copolymer," *Journal of the American Chemical Society* 131 (2009): 7484–7485, https://doi.org/10.1021/ja810046q.

18. M. Overduin and B. Klumperman, "Advancing Membrane Biology With Poly(Styrene–Maleic Acid)-Based Native Nanodiscs," *European Polymer Journal* 110 (2019): 63–68, https://doi.org/10.1016/j.eurpolymj.2018.11.015.

19. A. O. Oluwole, J. Klingler, B. Danielczak, et al., "Formation of Lipid-Bilayer Nanodiscs by Diisobutylene/Maleic Acid (DIBMA) Copolymer," *Langmuir* 33 (2017): 14378–14388, https://doi.org/10.1021/acs.langmuir.7b03742.

20. A. A. Gulamhussein, R. Uddin, B. J. Tighe, D. R. Poyner, and A. J. Rothnie, "A Comparison of SMA (Styrene Maleic Acid) and DIBMA (Di-Isobutylene Maleic Acid) for Membrane Protein Purification," *Biochimica Et Biophysica Acta (BBA)—Biomembranes* 1862 (2020): 183281, https://doi.org/10.1016/j.bbamem.2020.183281.

21. R. Adao, P. F. Cruz, D. C. Vaz, et al., "DIBMA Nanodiscs Keep Alpha-Synuclein Folded," *Biochimica Et Biophysica Acta (BBA)—Biomembranes* 1862 (2020): 183314, https://doi.org/10.1016/j.bbamem.2020.183314.

22. B. Danielczak, A. Meister, and S. Keller, "Influence of Mg(2+) and Ca(2+) on Nanodisc Formation by Diisobutylene/Maleic Acid (DIBMA) Copolymer," *Chemistry and Physics of Lipids* 221 (2019): 30–38, https://doi.org/10.1016/j.chemphyslip.2019.03.004.

23. N. Voskoboynikova, E. G. Margheritis, F. Kodde, et al., "Evaluation of DIBMA Nanoparticles of Variable Size and Anionic Lipid Content as Tools for the Structural and Functional Study of Membrane Proteins," *Biochimica Et Biophysica Acta (BBA)—Biomembranes* 1863 (2021): 183588, https://doi.org/10.1016/j.bbamem.2021.183588.

24. S. C. Lee, T. J. Knowles, V. L. Postis, et al., "A Method for Detergent-Free Isolation of Membrane Proteins in Their Local Lipid Environment," *Nature Protocols* 11 (2016): 1149–1162, https://doi.org/10.1038/nprot.2016.070.

25. N. L. Pollock, M. Rai, K. S. Simon, et al., "SMA-PAGE: A New Method to Examine Complexes of Membrane Proteins Using SMALP Nano-Encapsulation and Native Gel Electrophoresis," *Biochimica Et Biophysica Acta (BBA)—Biomembranes* 1861 (2019): 1437–1445, https://doi.org/10.1016/j.bbamem.2019.05.011.

26. N. G. Brady, M. Li, Y. Ma, J. C. Gumbart, and B. D. Bruce, "Non-Detergent Isolation of a Cyanobacterial Photosystem I Using Styrene Maleic Acid Alternating Copolymers," *RSC Advances* 9 (2019): 31781–31796, https://doi.org/10.1039/c9ra04619d.

27. N. G. Brady, S. Qian, J. Nguyen, H. M. O'Neill, and B. D. Bruce, "Small Angle Neutron Scattering and Lipidomic Analysis of a Native, Trimeric PSI-SMALP From a Thermophilic Cyanobacteria," *Biochimica*

et Biophysica (BBA)—Bioenergetics 1863 (2022): 148596, https://doi.org/10.1016/j.bbabio.2022.148596.

28. O. I. Korotych, T. T. Nguyen, B. C. Reagan, T. M. Burch-Smith, and B. D. Bruce, "Poly(Styrene-Co-Maleic Acid)-Mediated Isolation of Supramolecular Membrane Protein Complexes From Plant Thylakoids," *Biochimica et Biophysica (BBA)—Bioenergetics* 1862 (2021): 148347, https://doi.org/10.1016/j.bbabio.2020.148347.

29. B. D. Bruce, "The Role of Lipids in Plastid Protein Transport," *Plant Molecular Biology* 38 (1998): 223–246, https://doi.org/10.1023/A:1006094308805.

30. L. Boudiere, M. Michaud, D. Petroutsos, et al., "Glycerolipids in Photosynthesis: Composition, Synthesis and Trafficking," *Biochimica Et Biophysica Acta* 1837 (2014): 470–480, https://doi.org/10.1016/j.bbabio.2013.09.007.

31. K. Kobayashi, "Role of Membrane Glycerolipids in Photosynthesis, Thylakoid Biogenesis and Chloroplast Development," *Journal of Plant Research* 129 (2016): 565–580, https://doi.org/10.1007/s10265-016-0827-y.

32. K. Awai, "Thylakoid Development and Galactolipid Synthesis in Cyanobacteria," *Sub-Cellular Biochemistry* 86 (2016): 85–101, https://doi.org/10.1007/978-3-319-25979-6_4.

33. K. Gounaris and J. Barber, "Monogalactosyldiacylglycerol—The Most Abundant Polar Lipid in Nature," *Trends in Biochemical Sciences* 8 (1983): 378–381, https://doi.org/10.1016/0968-0004(83)90366-3.

34. K. Funai, S. A. Summers, and J. Rutter, "Reign in the Membrane: How Common Lipids Govern Mitochondrial Function," *Current Opinion in Cell Biology* 63 (2020): 162–173, https://doi.org/10.1016/j.ceb.2020.01.006.

35. C. L. Ladner-Keay, R. J. Turner, and R. A. Edwards, "Fluorescent Protein Visualization Immediately After Gel Electrophoresis Using an in-Gel Trichloroethanol Photoreaction With Tryptophan," *Methods in Molecular Biology* 1853 (2018): 179–190, https://doi.org/10.1007/978-1-4939-8745-0_22.

36. C. L. Ladner, J. Yang, R. J. Turner, and R. A. Edwards, "Visible Fluorescent Detection of Proteins in Polyacrylamide Gels Without Staining," *Analytical Biochemistry* 326 (2004): 13–20, https://doi.org/10.1016/j.ab.2003.10.047.

37. A. Chopra, W. G. Willmore, and K. K. Biggar, "Protein Quantification and Visualization via Ultraviolet-Dependent Labeling With 2,2,2-Trichloroethanol," *Scientific Reports* 9 (2019): 13923, https://doi.org/10.1038/s41598-019-50385-9.

38. D. Glueck, A. Grethen, M. Das, et al., "Electroneutral Polymer Nanodiscs Enable Interference-Free Probing of Membrane Proteins in a Lipid-Bilayer Environment," *Small* 18 (2022): e2202492, https://doi.org/10.1002/smll.202202492.

39. D. Kazmin, R. A. Edwards, R. J. Turner, E. Larson, and J. Starkey, "Visualization of Proteins in Acrylamide Gels Using Ultraviolet Illumination," *Analytical Biochemistry* 301 (2002): 91–96, https://doi.org/10.1006/abio.2001.5488.

40. C. L. Ladner, R. A. Edwards, D. C. Schriemer, and R. J. Turner, "Identification of Trichloroethanol Visualized Proteins From Two-Dimensional Polyacrylamide Gels by Mass Spectrometry," *Analytical Chemistry* 78 (2006): 2388–2396, https://doi.org/10.1021/ac051851y.

41. C. L. Ladner, R. J. Turner, and R. A. Edwards, "Development of Indole Chemistry to Label Tryptophan Residues in Protein for Determination of Tryptophan Surface Accessibility," *Protein Science* 16 (2007): 1204–1213, https://doi.org/10.1110/ps.062728407.

42. P. Jordan, P. Fromme, H. T. Witt, O. Klukas, W. Saenger, and N. Krauss, "Three-Dimensional Structure of Cyanobacterial Photosystem I at 2.5 A Resolution," *Nature* 411 (2001): 909–917, https://doi.org/10.1038/35082000.